Co-chaperone BAG3 enters autophagic pathway via its interaction with microtubule associated protein 1 light chain 3 beta

Hagen Körschgen[1] | Marius Baeken[2] | Daniel Schmitt[1] | Heike Nagel[1] | Christian Behl[1]

[1]The Autophagy Lab, Institute of Pathobiochemistry, University Medical Center of the Johannes Gutenberg University Mainz, Mainz, Germany

[2]Nucleic Acid Chemistry and Engineering Unit, Okinawa Institute of Science and Technology, Okinawa, Japan

Correspondence
Christian Behl, Institute of Pathobiochemistry, University Medical Center of the Johannes Gutenberg University Mainz, Duesbergweg 6, D-55099 Mainz, Germany.
Email: cbehl@uni-mainz.de

Abstract

The co-chaperone BAG3 is a hub for a variety of cellular pathways via its multiple domains and its interaction with chaperones of the HSP70 family or small HSPs. During aging and under cellular stress conditions in particular, BAG3, together with molecular chaperones, ensures the sequestration of aggregated or aggregation-prone ubiquitinated proteins to the autophagic-lysosomal system via ubiquitin receptors. Accumulating evidence for BAG3-mediated selective autophagy independent of cargo ubiquitination led to analyses predicting a direct interaction of BAG3 with LC3 proteins. Phylogenetically, BAG3 comprises several highly conserved potential LIRs, LC3-interacting regions, which might allow for the direct targeting of BAG3 including its cargo to autophagosomes and drive their autophagic degradation. Based on pull-down experiments, peptide arrays and proximity ligation assays, our results provide evidence of an interaction of BAG3 with LC3B. In addition, we could demonstrate that disabling all predicted LIRs abolished the inducibility of a colocalization of BAG3 with LC3B-positive structures and resulted in a substantial decrease of BAG3 levels within purified native autophagic vesicles compared with wild-type BAG3. These results suggest an autophagic targeting of BAG3 via interaction with LC3B. Therefore, we conclude that, in addition to being a key co-chaperone to HSP70, BAG3 may also act as a cargo receptor for client proteins, which would significantly extend the role of BAG3 in selective macroautophagy and protein quality control.

KEYWORDS
BAG3, BAG3-mediated autophagy, Bcl2-associated athanogene 3, LC3, LIR

1 | INTRODUCTION

Maintaining proteostasis, particularly under cellular stress conditions that promote protein misfolding or degradation, is crucial for a functional proteome. Accordingly, sophisticated protein quality control mechanisms have evolved, and eukaryotic cells govern the disposal of dysfunctional proteins via the ubiquitin–proteasome system and the autophagosome–lysosome pathway. Consequently, it is essential to specifically select such proteins that need to be degraded.

Molecular chaperones, such as HSPA (HSP70s) or HSPB (small HSPs), are able to identify and bind disordered or hydrophobic regions

---

Hagen Körschgen, Marius Baeken and Daniel Schmitt contributed equally to this work and should be considered joint first author.

of unfolded proteins.[1,2] In a coordinated multiprotein complex with other chaperones and co-chaperones, those ligands are either refolded to their native state or, if not achievable, sequestered for degradation.[3–5] Here, the cytoplasmic co-chaperone BAG3 (Bcl-2 associated athanogene 3) mediates a translocation to perinuclear sites to transfer the cargo to the autophagic pathway.[6–8] Together with HSP70, its multidomain structure—consisting of the WW, PxxP and BAG domains, as well as its IPV and 14-3-3 motifs—enable BAG3 to serve as a hub for proteotoxicity-induced signaling.[9] The cargo of small HSPs and HSP70s attaches to BAG3 via the IPV motifs and the BAG domain, respectively.[7,10,11]

Canonically, BAG3-mediated selective macroautophagy (referred to as autophagy), requires the recognition of the cargo's ubiquitination status.[12] Ubiquitinated protein aggregates are recognized by adapters/receptors like NBR2 (Neighbor Of BRCA1), OPTN (Optineurin), or p62/SQSTM1 (Sequestosome 1) and targeted to phagophores via interaction with lipidated ATG8 proteins.[13–15]

In most mammals, six genes encode for members of ATG8-family proteins. Three genes each encode for variants of either microtubule-associated proteins 1A/1B light chain 3 (LC3A, LC3B and LC3C) or γ-aminobutyric acid receptor-associated proteins (GABARAP, GABARAPL1 and GABARPL2). Conjugated to phosphatidylethanolamine, these are the only membrane-anchored representatives of ubiquitin-like proteins.[16]

Most ATG8-interacting proteins comprise an ATG8-interacting motif (AIM, LC3 interacting region [LIR] or GABARAP interacting motif [GIM]), which is characterized by an aromatic residue and a branched hydrophobic sidechain ([F/W/Y]$_0$XX[L/I/V]$_3$) separated by two amino acids.[17] In many cases, this core motif is flanked by acidic or polar residues, predominantly N-terminally.[18] Accordingly, the phosphorylation of the polar residues in many ligands positively modulates their binding

to LC3.[19–21] Additional, non-canonical binding motifs that lack the aromatic residue interacting with the hydrophobic pocket (HP1) of LC3 proteins, as well as the binding via accessory interaction sites have been described recently.[22–25] In the past years, few studies addressed the binding preferences and specificity of ATG8s.[21,26,27] Thus far, some ligand preferences have been characterized.[28]

The different binding modes and the varying preferences of ATG8 proteins illustrate the complexity in regulating the sequestration of autophagic cargo. Apart from the bona fide autophagy receptor p62, which links ubiquitinated cargo with ATG8 proteins, emerging data also indicate ubiquitin-independent autophagic degradation of cargo sequestrated by BAG3.[8,29] A direct interaction of BAG3 with ATG8 proteins might explain this degradation route. Indeed, our previous in silico analyses have identified five potential LIR motifs in BAG3 that are conserved within the craniotes.[30] In human BAG3, these include Y^{86}PQL^{89}, Y^{93}IPI^{96}, Y^{205}ISI^{208}, Y^{247}HKI^{250} and Y^{451}LMI^{454}.

Here, we further investigated BAG3 for its interaction with LC3 proteins. Our results strongly suggest a specificity of these in silico identified LIRs for LC3B. Inactivation of these LIRs significantly reduced BAG3 levels in autophagic vesicles. These findings suggest the potential function of BAG3 as an adapter for non-ubiquitinated autophagic cargo in addition to its co-chaperone activity, significantly expanding the role of BAG3 in selective autophagy.

2 | MATERIALS AND METHODS

2.1 | Antibodies

See Table 1 for the list of antibodies used.

TABLE 1 List of all antibodies used.

Antigen	Species	Distributor	Cat. no.	Dilution		
				Blot	IF (PLA)	Flow Cyt
BAG3	Mouse	Abnova	H00009531-M01A	1:1000	1:200 (1:200)	
	Rabbit	Proteintech Group, Inc.	10 599-1-AP	1:1000	(1:200)	
GABARAP/L1/L2-PE	Rabbit	Abcam	ab223948			4 µg/mL
GABARAP/L1/L2-APC	Rabbit	Abcam	ab223949			2 µg/mL
HSP70	Mouse	Enzo Life Sciences	ADI-SPA-810		(1:200)	
GABARAP	Rabbit	Cell Signaling Technology	13 733	1:1000		
GABARAPL1	Rabbit	Cell Signaling Technology	26 632	1:1000		
GABARAPL2	Rabbit	Cell Signaling Technology	14 256	1:1000		
MAP1LC3A	Rabbit	Cell Signaling Technology	4599	1:500	1:200	
MAP1LC3B	Mouse	nanoTools	0260-100/LC3-2G6	1:1000		
	Rabbit	Merck	L7543	1:1000	1:200 (1:200)	
MAP1LC3C	Rabbit	Abcam	ab150367	1:500	1:200	
NBR1	Mouse	Abnova	H00004077-M01		(1:200)	
p62 (SQSTM1)	Guinea pig	PROGEN Biotechnik	GP62-C	1:1000		
Tubulin	Mouse	Merck	T9026	1:1000		

Abbreviation: PLA, proximity ligation assay.

2.2 | Cell culture and treatment

HeLa cells (Clone HR5-CL11, verified via cell line authentication; Eurofins Genomics, Ebersberg, Germany) were used to establish a BAG3-deficient cell line via CRISPR-Cas9 technology[31] using 5′-GACCGGCTGGCCCTTCTTCG-3′ as BAG3 gRNA. CRISPR/Cas success was verified via NGS (Laborarztpraxis Rhein-Main MVZ GbR, Frankfurt, Germany) for all three BAG3 alleles, confirming the premature termination of translation resulting in a nonfunctional protein. Cells were transfected with three different plasmids each encoding a unique U6 driven gRNA sequence and a CMV driven Cas9 nuclease. Forty-eight hours posttransfection, the cells were singularized into 96-well plates, and the knock-out was confirmed by sequencing and immunoblot analysis (Figure 1A). Cells were cultured in Dulbecco's Modified Eagle Medium (DMEM; gibco, 41965-039) supplemented with 10% (v/v) fetal bovine serum, 1 mM sodium pyruvate (gibco, 11360039) and 1% antibiotic/antimycotic solution (Merck, A5955). Medium was refreshed every 3 days during cultivation and every 24 h in an experimental setting. Cells were treated with stock solutions of MG-132 (Merck, 474 790), PYR-41 (Merck, 662 105) or Bafilomycin A1 (BafA1; Biozol, TOR-B110000) in dimethyl sulfoxide (DMSO) as specified.

2.3 | Autophagic vesicle purification

Autophagic vesicles were purified based on a novel purification method described previously.[32] At least 1×10^7 cells were collected using Trypsin/ethylenediaminetetraacetic acid (EDTA) and centrifuged at $306 \times g$ for 4 min. After resuspension in PBS supplemented with cOmplete™ EDTA-free (Roche), cell disruption was performed using a UP50H ultrasonic processor (Hielscher) for 3×2 s with an amplitude of 60%. Samples were then centrifuged at $3000 \times g$ for 10 min at 4°C, supernatants were collected and centrifuged at $18\,620 \times g$ for 1 h at 4°C. Pellets were washed and resuspended in PBS and subsequently incubated with 4 μg/mL of phycoerythrin (PE)-conjugated GABARAP/GABARAPL1/GABARAPL2 antibody (Abcam, ab223948) for 1 h. The samples were centrifuged again with $18\,620 \times g$ for 1 h at 4°C, pellets were washed and resuspended in PBS. For autophagic vesicle sorting, a BD FACSAria III SORP (BD Biosciences) equipped with a 70 μm nozzle and a 1.0 forward scatter (FSC) neutral density filter was used. The compartment containing autophagic vesicles was first established using an FSC/side scatter (SSC) plot on a logarithmic scale, followed by a doublet discrimination gate using SSC-A/W. Autophagic vesicles were defined as PE-positive events (488 nm, BP 530/30), whose positivity was conducted according to the background given by an unstained negative control. Vesicle sorting was achieved using minimum speed (flow rate <3.0) maintaining <19 000 events per second. Analysis was performed using FlowJo v10.6.1 (BD Biosciences). Proteins of isolated autophagic vesicles were analyzed using a methanol/chloroform (2:1) precipitation protocol and subsequent resuspension in urea buffer (8 M urea and 4% [w/v] CHAPS in 30 mM Tris [pH 8.5 with HCl]), including EDTA-free

protease inhibitor. For immunoblot quantification, we analyzed 2 million autophagic vesicles each by normalizing to the initial amount of tubulin and expression level of wild-type BAG3 and ΔLIR-BAG3, respectively.

2.4 | Flow cytometric analysis of autophagic vesicles

Approximately 5×10^6 cells were prepared for cytometric analysis as described above using 2 μg/mL of APC-conjugated GABARAP/GABARAPL1/GABARAPL2 antibody (Abcam, ab223949). Autophagic vesicles were defined as APC-positive (640 nm, BP 670/30) events according to the background given by an unstained negative control. BAG3-EGFP (enhanced green fluorescent protein) was defined as EGFP-positive (488 nm, BP 530/30) events and positivity was conducted according to the background given by a negative control transfected with an empty vector as well as stained with an APC-conjugated GABARAP/GABARAPL1/GABARAPL2 antibody. Analyses were performed using the LSRFortessa SORP (BD Biosciences) flow cytometer and subsequently analyzed with FlowJo v10.6.1 (BD Biosciences).

2.5 | Immunoprecipitation

Cells were lysed in immunoprecipitation buffer (50 mM Tris, pH 7.4, 150 mM NaCl, 2 mM Na_2EDTA, 1 mM Na_4EGTA, 10% glycerol, 1% Triton X-100, 1 mg/mL cOmplete™ EDTA-free) and passed three times through a 23G needle. Protein concentration was determined using BCA assay (Thermo Fisher Scientific, 23225). The lysate (500 μg) was precleared with Pierce™ Protein A/G magnetic beads (ThermoFisher Scientific, 88 802), incubated with 2 μL anti-BAG3 antibody (Proteintech, 10599-1-AP) at 4°C and precipitated with fresh beads. After three washing steps, elution was accomplished via reducing SDS loading buffer. Samples were separated via SDS-PAGE and analyzed via immunoblotting.

2.6 | Colocalization analysis by immunofluorescence microscopy

BAG3-deficient HeLa cells were cultured on glass cover slips and treated as indicated. Cells were then fixed with 4% formaldehyde in PBS (Carl Roth, P087.5), permeabilized with 90% (v/v) methanol and blocked using PBS + 3% (w/v) bovine albumin. Antibodies were incubated as specified in PBS + 1% (w/v) albumin. After incubation with primary antibodies, cells were incubated with cyanine (Cy3, Cy5)-conjugated antibodies (Jackson ImmunoResearch) as well as DAPI (4′,6-diamidino-2-phenylindole). Stained cells were imaged via the Opera Phenix High-Content Screening System (Perkin-Elmer). For evaluation of colocalization, single slides (40× magnification) with approximately 15 cells per image were acquired of at least 5 randomly

chosen optical fields from three independent biological replicates. BAG3 and LC3 spots were detected using the Harmony High-Content Imaging and Analysis software (Perkin-Elmer) within the cytoplasm excluding positive signals in the nucleus. Colocalization was calculated for up to 200 000 single BAG3 spots for each condition and cell line for three biological replicates as colocalizing BAG3 spot area [px^2] in relation to total BAG3 spot area [px^2] with due regard to the background given by a negative control transfected with an empty vector.
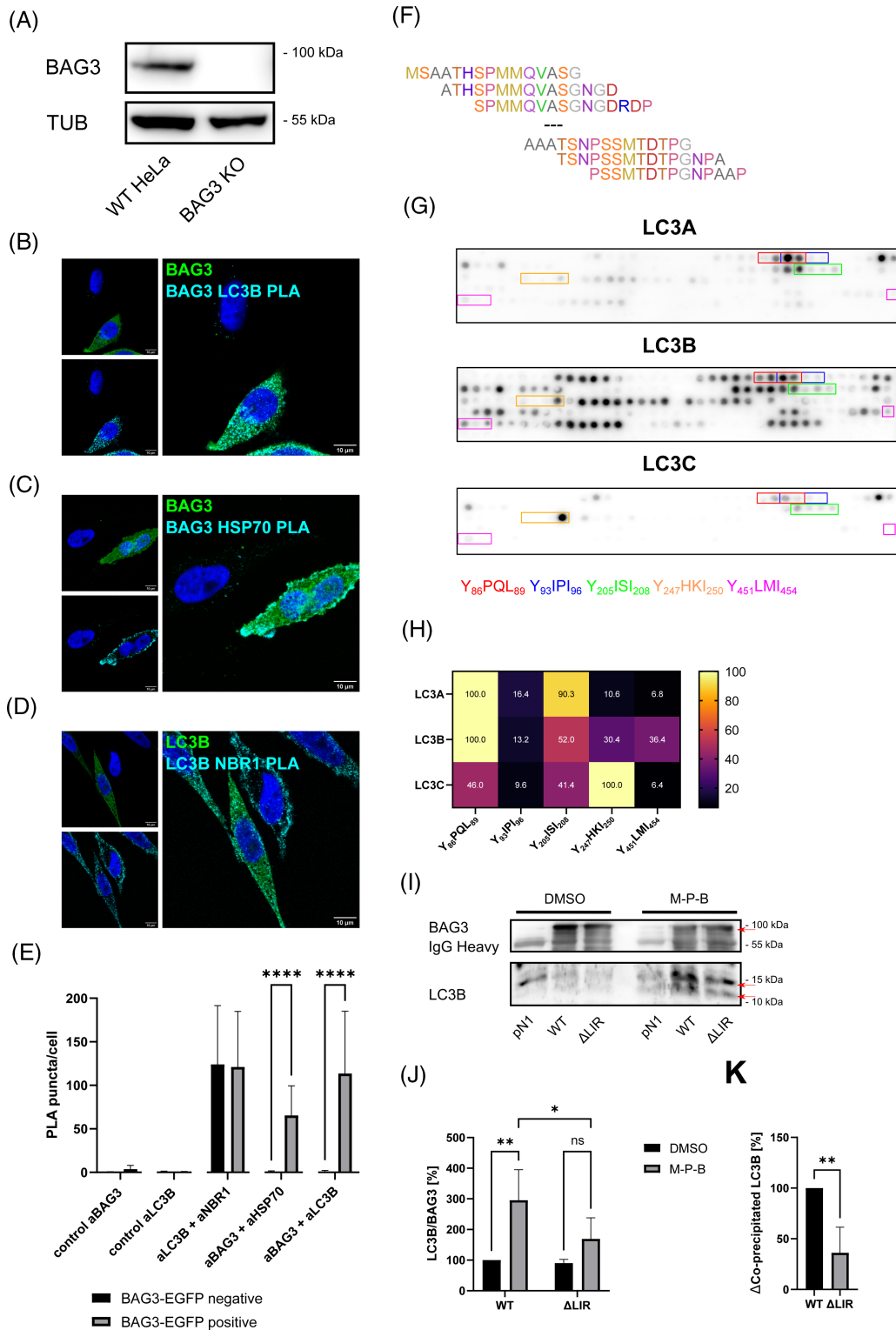

FIGURE 1 Legend on next page.

The quantitative levels of BAG3 within LC3B-positive structures were defined as the mean area [px^2] of up to 70 000 single colocalizing BAG3 spots. All additional Plot profiles were created using FIJI v2.1.0[33] showing the gray value of the different fluorescence channels depending on the distance of a given region of interest.

2.7 | Peptide array

Spot synthesis for peptide array of human BAG3 (15mer peptides, three residues shift per spot, N-terminally acetylated) on cellulose membrane was acquired from Intavis Peptides Services (Tübingen, Germany). Protein binding was performed according to the manufacturer's specification using heterologously expressed and glutathione S-transferase (GST)-tagged LC3s (LC3A, Novusbio, H00084557-P01; LC3B, Novoprolabs, 509 467; LC3C, Abnova, H00440738-P01) at 2 μg/mL. Binding of the proteins was evaluated using an anti-GST-horseradish peroxidase conjugate (GE Healthcare, RPN1236). For comparative evaluation of affinities, the signal intensities of the respective LIR motif-containing peptides were averaged and normalized to the averaged intensity of the most intense motif. In the case of peptides containing two LIR motifs, the signals from overlapping peptides were excluded from evaluation.

2.8 | Plasmids and transfection

BAG3-deficient HeLa cells were transiently transfected via calcium phosphate precipitation. Transfected cells were washed 24 h posttransfection and the medium was refreshed. Treatment was administered in an appropriate manner to allow harvesting the cells 48 h after transfection. Expression constructs of wild-type human BAG3 and C-terminal EGFP-tagged BAG3 were used as previously published.[6] Single point LIR mutants and eventually ΔLIR-BAG3 (Y^{86}S, Y^{93}S, Y^{205}S, Y^{247}S, I^{454}T) were generated using, the Quik-Change Lightning Site-Directed Mutagenesis Kit (Agilent, 210 518) according to the manufacturer's instructions (Table 2). Mutagenesis was confirmed via sequencing.

2.9 | Proximity ligation assay

In situ protein–protein interaction was evidenced using Duolink® proximity ligation assay (PLA; Merck, DUO920082, DUO92004, DUO92008). Cells were fixed with formaldehyde and permeabilized using ice-cold 90% methanol. The sample preparation was conducted according to the manufacturer's protocol with an amplification time of 150 min. Stained cells were imaged with a Zeiss LSM710 confocal microscope. Puncta per cell of at least three biological replicates were counted using ImageJ for three randomly selected areas with both EGFP-positive and -negative cells and statistically analyzed as indicated.

2.10 | Immunoblotting

Samples were mixed with reducing SDS-loading buffer, incubated for 5 min at 98°C and subjected to SDS-PAGE. Gels were then blotted onto nitrocellulose membranes and subsequently incubated in/blocked with 5% nonfat dried milk powder dissolved in Tris-buffered saline (TBS)-T (0.05% Tween-20) for 1 h at room temperature. Membranes were probed with the required primary (1:X00 in TBS-T) and peroxidase-conjugated secondary antibodies (1:1000 in TBST) as indicated. Detection was performed with an Amersham Imager 600 system (GE Scientific).

2.11 | In silico modeling

In silico modeling of ΔLIR-BAG3 based on wild-type BAG3 (AlphaFold model) was performed using SWISS-MODEL.[34] The superposition of the two models was created using matchmaker tool implemented in UCSF Chimera.[35]

FIGURE 1 Analysis of BAG3–LC3B interaction. (A) BAG3 deficiency on protein level in HeLa cells confirmed by immunoblot. (B–D) Representative images of proximity ligation assay (PLA) of BAG3–LC3B interaction (cyan) (B), BAG3–HSP70 interaction (C) and LC3B–NBR1 interaction (D). All PLA were performed on BAG3-deficient cells transiently transfected with human BAG3–EGFP and treated with MG-132 (10 h, 25 μM), Bafilomycin A1 (4 h, 2 μM) and PYR-41 (4 h, 12.5 μM). Displayed are representative images obtained from three independent experiments. Magnification: 100×. Scale bar: 10 μm. (E) Analysis of proximity ligation puncta per cell of (B–D) and of Figure S1A, Statistical significances were reported after two-way ANOVAs followed by a Benjamini–Hochberg post hoc tests. "****" indicates $p \leq 0.0001$. (F) Exemplary of the first and last three oligopeptides part of the BAG3 peptide array. With each peptide the primary structure of the oligopeptide shifts by three amino acids towards the C-terminus. (G) Membranes of the BAG3 peptide arrays incubated with the indicated recombinant human glutathione S-transferase (GST)-tagged LC3 protein. LC3 binding was detected using an anti-GST antibody. Oligopeptides containing the predicted LIR motif are highlighted with a unique color. (H) Heatmap comparing mean signal intensity of all peptides containing each LIR of the arrays displayed in G. The motif with the strongest mean signal intensity was defined as 100%. (I) Immunoprecipitations of BAG3-deficient cells transfected with empty vector (pN1), wild type (WT)-BAG3 or ΔLIR-BAG3. Cells were treated for 8 h with MG-132 (25 μM), PYR-41 (12.5 μM) and Bafilomycin A1 (2 μM) (M-P-B) or dimethyl sulfoxide (DMSO); 48 h posttransfection whole cell lysates were obtained and immunoprecipitated using an anti-BAG3 antibody. Red arrows indicate which signals were quantified. (J) LC3B/BAG3 ratio for WT-BAG3 and ΔLIR-BAG3, with and without treatment obtained from I (four independent experiments). (K) Accumulation of co-precipitated LC3B by M-P-B treatment in cells transfected with WT-BAG3 or ΔLIR-BAG3 obtained from I (four independent experiments).

TABLE 2   List of primers used for mutagenesis.

BAG3 mutagenesis	Forward primer (5′-3′)	Reverse primer (5′-3′)
$Y^{86}PQL^{89} \rightarrow S^{86}PQL^{89}$	AGGCCACCCTGTGAGCCCCCAGCTCCGA	TCGGAGCTGGGGGCTCACAGGGTGGCCT
$Y^{93}IPI^{96} \rightarrow S^{93}IPI^{96}$	CCAGCTCCGACCAGGCAGCATTCCCATTCCTGTG	CACAGGAATGGGAATGCTGCCTGGTCGGAGCTGG
$Y^{205}ISI^{208} \rightarrow S^{205}ISI^{208}$	GCTCCCGCGGGGGAGCATCTCCATTCCG	CGGAATGGAGATGCTCCCCCGCGGGAGC
$Y^{247}HKI^{250} \rightarrow S^{247}HKI^{250}$	ACCCACCAGCCTGTGAGCCACAAGATCCAGGG	CCCTGGATCTTGTGGCTCACAGGCTGGTGGGT
$Y^{451}LMI^{454} \rightarrow Y^{451}LMT^{454}$	CTTTGGTCAAATACTCTTCGGTCAT CAGGTACTTTTTGTCAGTC	GACTGACAAAAGTACCTGATGACCGAA GAGTATTTGACCAAG

2.12 | Statistical methods

Graphs and statistics were assembled using GraphPad Prism 9 (Graph-Pad Software, Inc.) All statistical analyses were performed according to normal distribution and variance differences by one-way or two-way analysis of variance (ANOVA) followed by original Benjamini and Hochberg post hoc tests. The results display mean ± standard deviation (SD) or standard error of the mean (SEM) as indicated. Statistical significance was accepted at a level of $p < 0.05$ (p-value ≤ 0.05 = *, ≤0.01 = **, ≤0.001 = ***, ≤0.0001 = ****).

3 | RESULTS

3.1 | BAG3 interacts with LC3B in situ and favors the $Y^{86}PQL^{89}$ motif in vitro

We generated a BAG3-deficient HeLa cell line using a CRISPR/Cas9 approach to provide a cell line with a defined background. The cells were characterized both at the genetic and protein level (Figure 1A). First, we investigated the potential interaction of BAG3 with the bona fide ATG8 protein LC3B in cellulo by proximity ligation. This assay employs immunodetection coupled with an amplification of DNA probes to detect the proximity (max. 40 nm distance) of two immuno-labeled proteins. In approximation, this method only uncovers direct interactions of two different proteins in situ. We were thus able to identify an interaction between BAG3 and LC3B using BAG3-EGFP overexpression in a BAG3-deficient background (Figure 1B,E). We treated the cells with MG-132 to inhibit proteasomal degradation and induce the BAG3-mediated selective autophagy pathway, and additionally treated with BafA1 to raise the total quantity of autophagic vesicles. Furthermore, we incubated cells with PYR-41[36] to diminish ubiquitination. Negative controls with the single antibodies against BAG3 and LC3B only (Figure S1A), and the positive controls with well-described interaction partners—such as HSP70 for BAG3 and NBR1 for LC3B (Figure 1C,D)—validated the method for detecting the binding of BAG3 to LC3B in situ. The evidence of a BAG3-HSP70 interaction is restricted only to cells displaying BAG3-EGFP expression, whereas the LC3B–NBR1 interaction is independent of BAG3 expression (Figure 1C,D). We also summarized the analysis of puncta per cell of the proximity ligation and its statistical evaluation (Figure 1E). Accordingly, detection of the BAG3-LC3B complex, which

also occurred in BAG3-positive cells only, is proof of principle for an in cellulo interaction.

Subsequently, before we evaluated which of the putative LIR motifs is functional, we performed an initial immunoprecipitation assay to verify which of the human ATG8 paralogs binds to wild-type BAG3. To this end, cells were treated with BafA1 and PYR-41 to induce BAG3-mediated selective autophagy and enhance the likelihood of binding. Interestingly, we found BAG3 to interact with all LC3 proteins, but with none of the GABARAP proteins (Figure S1C). We furthermore verified that the PYR-41 treatment did not disturb the autophagic flux in any relevant way (Figure S1D). Based on these data, we excluded the GABARAP proteins in subsequent experiments.

Next, we performed a BAG3 peptide array to assign binding to the five putative LIRs. Due to the lack of structural information on BAG3, a restriction to particular motifs in advance did not seem reasonable. We screened the amino acid sequence for binding regions using synthetic 15mer peptides by shifting each peptide by three residues (Figure 1F). The peptide array analysis did not indicate a clear binding preference for one single putative LIR motif (Figure 1G,H). For LC3A and especially LC3B, $Y^{86}PQL^{89}$ containing peptides revealed the highest affinity of the predicted LIRs. The next motif downstream, $Y^{93}IPI^{96}$, did not display any interaction for all LC3s, though a reliable evaluation was problematic due to overlapping with $Y^{86}PQL^{89}$ peptides. All three LC3 proteins exhibited a very weak binding to $Y^{205}ISI^{208}$-containing peptides. However, this motif might have a slight preference for LC3A. LC3C displayed the strongest interaction with one $Y^{247}HKI^{250}$ containing peptide, although here, as with LC3A and LC3B, only the one peptide containing this sequence at the free N-terminus was recognized. Accordingly, we cannot conclude that interactions with this motif are valid based on this approach. Binding to $Y^{451}LMI^{454}$, which is located within the BAG domain mediating the HSP70 interaction, was weak for LC3B and negligible for LC3A and LC3C. Apart from LC3C, whose interaction with the BAG3 peptides was almost exclusively limited to regions containing predicted LIRs, we observed pronounced interactions with peptides without classical LIR motifs for LC3A and especially for LC3B. However, unlike the putative canonic LIR motifs we have identified previously, these regions are either not conserved at all, or part of the WW or BAG domain, which likely dictate conservation of these regions.[30] Therefore, we assumed that these interactions are nonphysiological and may be caused by the high hydrophobicity of the spotted peptides. As this array did not provide a clear preference for a single LIR or

specificity for LC3 binding, we decided to employ a ΔLIR-BAG3 with disabled functionality of all putative LIR motifs. Within this ΔLIR-BAG3 mutant the tyrosine residues of the LIR motifs were changed to serine to retain the free hydroxyl group of the side chain. In the case of $Y^{451}LMI^{454}$, the isoleucine residue was mutated to a threonine, to reduce possible effects on the integrity and function of the BAG-domain. In silico modelling analyses also did not reveal any effect of these mutations on the structure of BAG3 (Figure S2).

Subsequently, we reassessed the interaction of BAG3 with the bona fide autophagy marker LC3B via immunoprecipitation. Overexpressed wild-type BAG3 and a ΔLIR-BAG3 mutant (Figure S1B), were immunoprecipitated under baseline and proteostasis stress conditions as indicated (Figure 1I). Under basal conditions, we only observed a weak, nonspecific coprecipitation of LC3B. Upon induction of BAG3-mediated autophagy via MG-132, PYR-41 treatment[36] to block ubiquitination, and BafA1 supplementation, we observed a strong increase of coprecipitating LC3B (Figure1I,J). This induction of interaction was completely lost in the ΔLIR-BAG3 mutant (Figure 1J). Indeed, calculating a Δ of coimmunoprecipitated LC3B between treated and untreated cells resulted in significantly less coimmunoprecipitated LC3B in the ΔLIR-BAG3 mutant (Figure 1K). Both results indicate the functionality of one or more LIR motifs in the interaction of BAG3 and LC3B.

3.2 | Inactivation of predicted LIR-motifs within BAG3 affects BAG3–LC3B interplay in cellulo

Next, we analyzed the colocalization dynamics for both wild-type BAG3 and ΔLIR-BAG3 under proteostasis stress conditions as this appeared to be necessary for the induction of the interaction with LC3B (Figure 1I). Here, we included LC3A and LC3C in addition to LC3B as the peptide array displayed a potential, although weak, interaction with $Y^{86}PQL^{89}$ or $Y^{205}ISI^{208}$ peptides (Figure 1G). Considering that other members of the LC3 protein family may compensate a potential loss of LC3B in the autophagic system, as we have previously reported,[37] this was of particular interest.

Our analysis of the relative colocalization area of wild-type BAG3 with LC3B under MG-132 treatment clearly demonstrated a superposition compared with the empty vector control. Compared with LC3A (Figure S3A,C) colocalization appeared to be elevated for LC3B (Figure 2A,C). For LC3C, we only observed interference at the level of the background given by the empty vector control, which was associated with a massive variation in the relative signal (Figure S3B,D). These results again suggest a certain selectivity for LC3B. Additional treatment with BafA1 slightly, but not significantly, elevated the relative area of colocalization with LC3A- or LC3B-positive structures (Figures 2C and 3C). The ΔLIR-BAG3 mutant exhibited an almost identical relative area of colocalization with LC3B as the wild type (Figure 2C). Here, we would like to mention that the colocalizing area itself did not provide any functional conclusion. For instance, merely the BafA1 treatment-induced increase in LC3-positive structures might intrinsically elevate the area of colocalization with ΔLIR-BAG3

without any functional significance. For assessing the functionality, solely the difference in the mean BAG3 concentration/intensity within LC3-positive structures is of significance. Accordingly, by considering parameters such as the mean BAG3 concentration (wild-type vs. ΔLIR), for example, the intensity within the colocalizing LC3 structures, we verified a functional component of the LIRs. In the first step, we compared the fluorescence intensity profiles of designated cell regions displaying a correlation of BAG3 and LC3B within all tested paradigms. However, the analyzed wild-type BAG3 fluorescence intensity closely correlated with the intensity peaks of LC3B (Figure 2B). This correlation was hardly evident for ΔLIR-BAG3. Especially upon BafA1 treatment, this became apparent. (Figure 2B). Subsequently, we analyzed the relative amount of wild-type BAG3 or ΔLIR-BAG3, respectively, within the LC3B-positive structures (Figure 2D). For wild-type BAG3, we observed a significant increase in the mean abundance of BAG3 colocalizing with LC3B-positive puncta following BafA1 treatment. This specific induction did not occur for ΔLIR-BAG3 (Figure 2D). Accordingly, since the BafA1 treatment in general did not provoke an accumulation, this enrichment of BAG3 within LC3B-positive structures has to depend on the specificity of one or more predicted LIR motifs. Next, we addressed the ensuing questions about the localization of BAG3 in autophagosomes and a LIR-dependent targeting into these structures by analyzing the content of isolated autophagic vesicles.

3.3 | BAG3 accumulates in isolated autophagic vesicles in a LIR-dependent manner

The recent establishment of a purification protocol in our lab[32] enabled us to extract and enrich intact native autophagic vesicles from cultured cells by means of a combination of successive centrifugations, an antibody-based fluorescence tagging of ATG8-positive structures and a subsequent sorting via flow cytometry (Figures 3A and S4). The different centrifugation/washing steps combined with fluorescent labeling of established autophagosomal marker proteins such as LC3B or GABARAP and, eventually, sorting via fluorescence-activated cell sorter effectively reduced the unlipidated form of LC3B accompanied by enriched levels of lipidated LC3B (Figure 3B). In accordance with Schmitt et al.[32] the specific detection and sorting of ATG8-positive structures eventually resulted in purified vesicles containing prominent autophagic markers such as LC3B and SQSTM1/p62 in the absence of cytosolic proteins (e.g., LC3B-I) or other contaminants like fragments of the cytoskeleton such as tubulin (Figure 3B). This enabled us to confirm a localization of BAG3 inside autophagic vesicles via flow cytometry. Using the specified protocol, we were able to confirm the presence of BAG3-EGFP in autophagosomes of transfected BAG3-deficient cells (Figure 3C). To test the LIR dependency of this autophagosome-localized BAG3 population, we transfected BAG3-deficient HeLa cells either with an empty vector (pN1), wild-type BAG3, or ΔLIR-BAG3. Figure 3D displays the total cell lysate (TL) applied for the autophagosomal isolation protocol. Despite minor variations, wild-type BAG3 and ΔLIR-BAG3 displayed
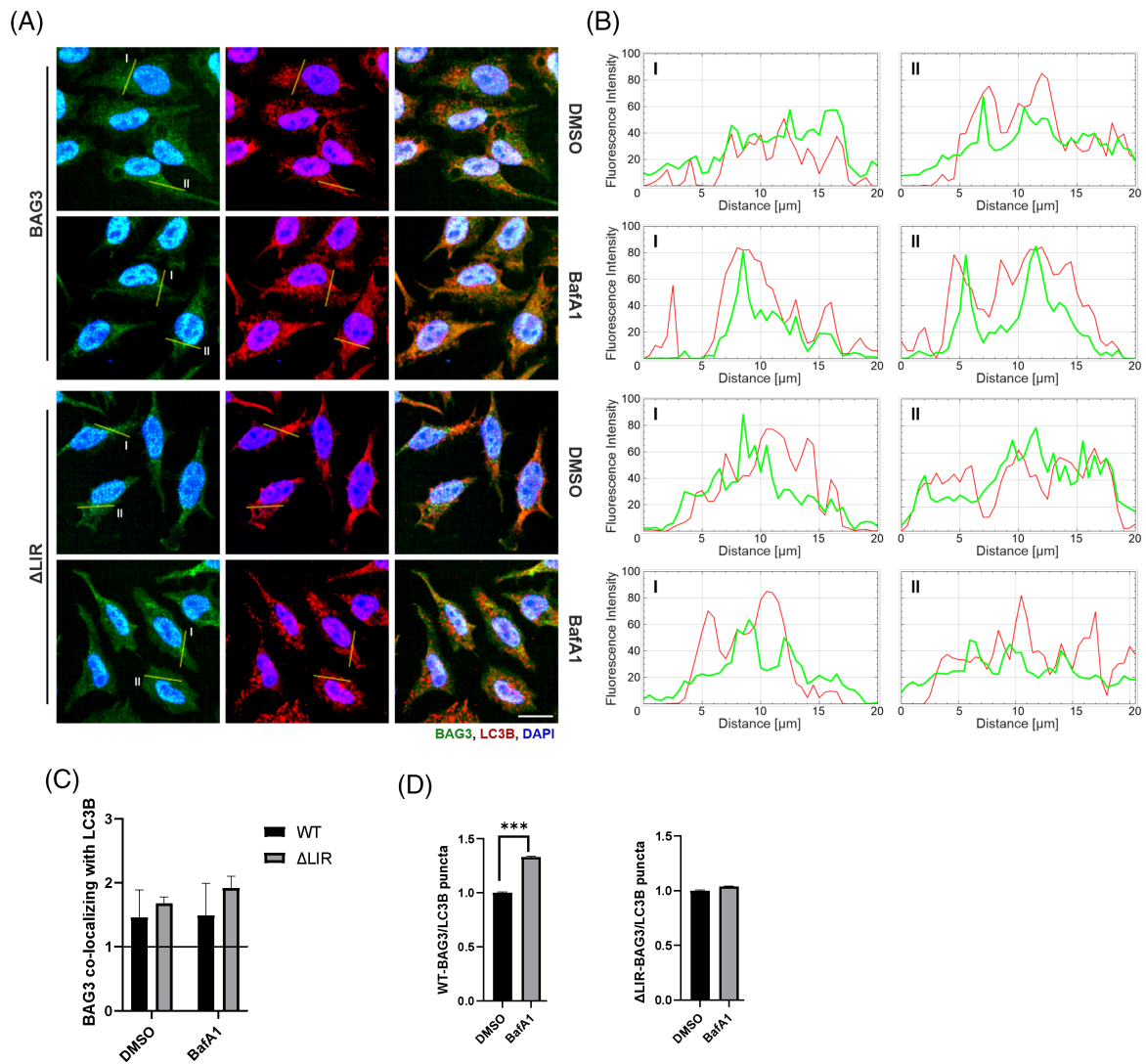
FIGURE 2 Colocalization analysis of wild type (WT) and ΔLIR-BAG3 with LC3B. (A) Representative images of BAG3-deficient cells overexpressing WT-BAG3 or ΔLIR-BAG3 upon MG-132 treatment (8 h, 10 μM) as well as dimethyl sulfoxide (DMSO; control) or Bafilomycin A1 (8 h, 2 μM) as indicated. Shown images are each representative for 15 slices of three independent experiments. BAG3 shown in green, the indicated LC3 in red. Nuclei were stained by DAPI. Magnification: 40×. Scale bar: 20 μm. (B) Fluorescence intensity profiles of (A) showing the gray values of the given channels within designated cell regions defined by distance [μm]. BAG3 shown in green, the indicated LC3 in red (C) Quantification of BAG3 colocalizing with indicated LC3 within the cells displayed in A. Shown is the relative area of BAG3 puncta colocalizing with LC3 normalized to the total BAG3 area. Statistics are depicted as mean ± SD of three independent experiments comprising up to 200 000 single BAG3 puncta for each condition and cell line; one-way ANOVA; no significant alterations were observed. (D) Relative mean area of colocalizing BAG3 puncta in LC3B-positive structures within the cells described in A. Statistics are depicted as mean ± SEM of up to 70 000 individual BAG3 puncta out of three independent experiments for each condition and cell line; one-way ANOVA followed by a Benjamini–Hochberg post hoc test; "*" indicates $p \leq 0.05$ and "***" $p \leq 0.001$.

similar expression levels and stability (Figure S1B). The specific gating strategy of the flow cytometry for the final separation of vesicles is illustrated in Figure S4. To define whether BAG3 accumulates in a LIR-dependent manner in autophagosomes, we comparatively analyzed the amount of wild-type BAG3 as well as ΔLIR-BAG3 in these autophagic vesicles. The results in Figure 3E clearly confirmed a high concentration of wild-type BAG3. Regarding an LIR-dependent targeting of BAG3 to autophagosomes, in a comparative analysis, we indeed observed that mutations of the LIR motifs resulted in a massive reduction of ΔLIR-BAG3 (Figure 3E,F) in isolated vesicles.

For the wild-type, additional treatment with PYR-41 effected a similar reduction of BAG3 in autophagic vesicles. Interestingly, we did not observe a reduction in ΔLIR-BAG3 levels in autophagic vesicles following PYR-41 treatment (Figure 3G). Since PYR-41 disables cellular ubiquitination capabilities, the reduction of BAG3 observed in autophagosomes, at first glance, may indicate at least a partial dependency on ubiquitination of cargo in order for BAG3 to act as an autophagy receptor. Likewise, the static behavior of ΔLIR-BAG3 (with its loss of function in all LIRs) when treated with PYR-41 further solidifies BAG3's potential function as an
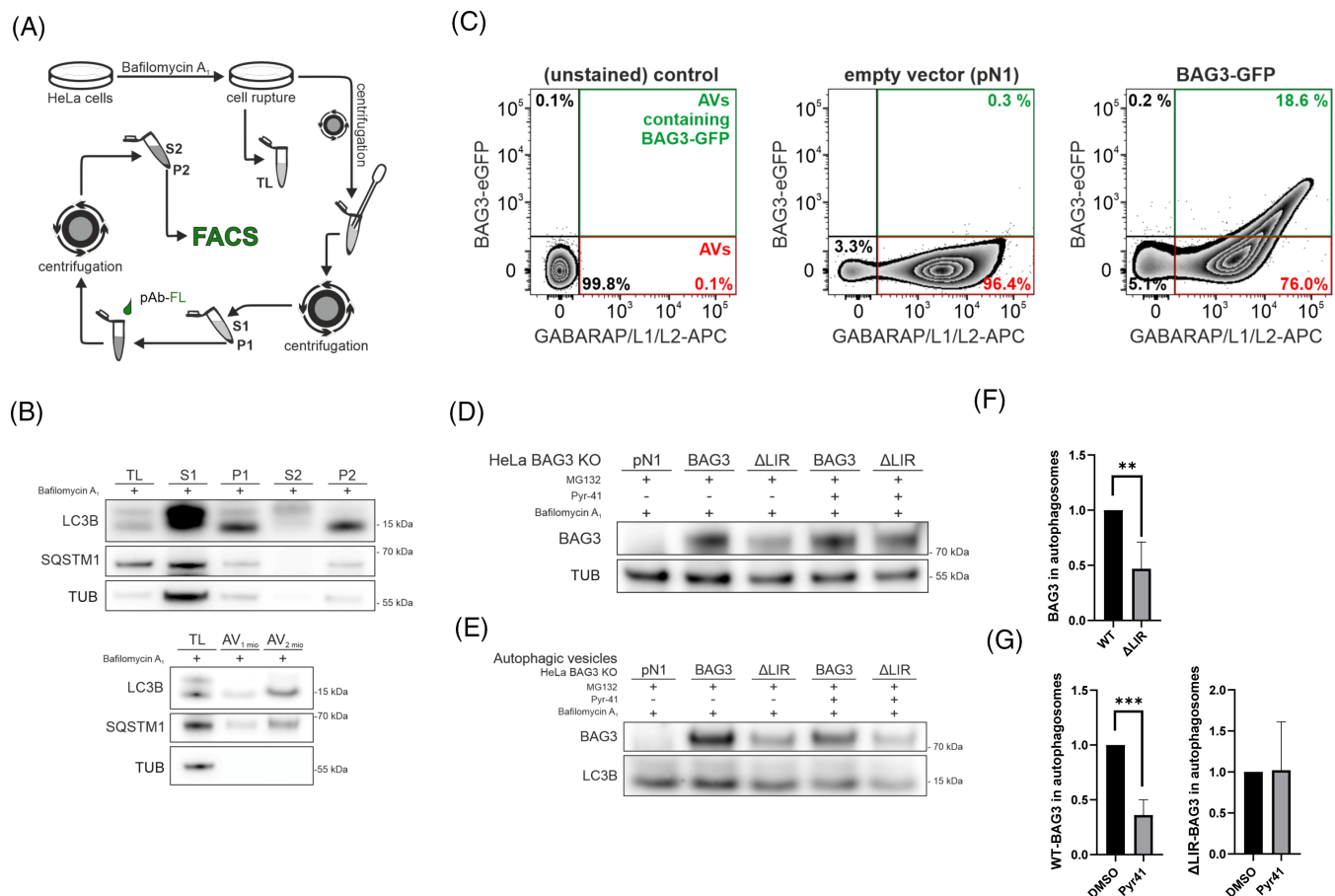
FIGURE 3 BAG3 in isolated native autophagic vesicles. (A) Schematic illustration of autophagic vesicle isolation. TL, total lysate; P1-2, pellet fractions; S1-2, supernatants; AV, autophagic vesicles. Gating strategy is shown in Figure S4. (B) Analysis of purification progress by immunoblot; fractions as indicated in (A); (C) Flow cytometric analysis of autophagic vesicles within BAG3-deficient cells overexpressing BAG3-EGFP in comparison to an unstained negative control as well as an empty vector (pN1) control. Cells were treated with MG-132 (8 h, 10 μM) and Bafilomycin A1 (8 h, 2 μM). Shown images are representative for three independent experiments. Gating strategy was set as indicated in Figure S4. (D) Immunoblot analysis of BAG3 in BAG3-deficient cells overexpressing WT-BAG3 or ΔLIR-BAG3 under MG-132 (8 h, 10 μM), Bafilomycin A1 (8 h, 2 μM) and PYR-41 (8 h, 12.5 μM) treatment as indicated. (E) BAG3 detection in autophagic vesicles isolated from BAG3-deficient cells described in (D). (F,G) Statistical analysis of (E). BAG3 levels were normalized to LC3B as a loading control as well as BAG3 levels in total lysates shown in (C) to compensate differences in transfection efficiency. Statistics are depicted as mean ± SD of three independent experiments; one-way ANOVA followed by a Benjamini–Hochberg post hoc test; "**" indicates $p \leq 0.01$ and "***" $p \leq 0.001$.

autophagy receptor. In summary, this approach confirmed a LIR-dependent accumulation of BAG3 in autophagic vesicles, with only minor amounts of ΔLIR-BAG3 present, likely representing BAG3 as cargo and not as a receptor.

4 | DISCUSSION

We have recently described the potential of BAG3 to serve as an autophagy receptor, since BAG3 features a surprisingly strong conservation of putative LIR motifs within the craniotes.[30] Therefore, we investigated an interaction of BAG3 with LC3 proteins, especially LC3B as a bona fide representative of ATG8 proteins, in vitro and in cellulo. Our data suggest a direct interaction of BAG3 especially with LC3B but barely with LC3C. All assays performed point to a LIR dependency of this interaction. The results of the peptide array only

provided evidence of an interaction with LC3A and LC3B for $Y^{86}PQL^{89}$ and $Y^{205}ISI^{208}$ containing peptides. The concomitant strong conservation of the other predicted LIRs, $Y^{93}IPI^{96}$ and $Y^{451}LMI^{454}$ throughout vertebrate evolution may also be explained by these LIR's being part of the first IPV motif essential for interaction with small HSPs or being part of the BAG domain, respectively. $Y^{205}ISI^{208}$ is equally a part of the second IPV motif. Interaction with an LC3 protein would presumably influence binding of small HSPs to BAG3. Possibly, this might represent a potential switch for interactions from HSPB6/8 to LC3 proteins. In particular, for LC3B, the peptide array exhibits presumably nonspecific non-LIR-containing interaction sites. Here, based on the recognized sequences, there are currently no data to elucidate whether these are noncanonical binding motifs or yet unknown interaction mechanisms. However, since these regions are not phylogenetically conserved, apart from conserved areas important for the PxxP or BAG domain, little data argues in favor of this avenue. Rather, the

signal may likewise partly be the result of unspecific binding due to the high frequency of hydrophobic residues[36] like in the PxxP domain within BAG3, which are also most frequent among the LC3s in LC3B, therefore, this was not further investigated. Whether these hydrophobic residues are accessible at all in the native protein is currently not evident due to the lack of structural information on BAG3. The effects of the ΔLIR-BAG3 mutant (Figure 1I–K) likewise indicate that such interactions, if they indeed exist within the intact BAG3 protein at all, play a minor role in comparison to the predicted LIRs.

Additionally, LC3C indicated a high affinity towards a $Y^{247}HKI^{250}$ containing peptide in the array (Figure 1G,H). Since we only detected the peptide containing this motif at the free N-terminus of the spotted peptide, the absence of interaction for the other three peptides containing $Y^{247}HKI^{250}$ might be due to a folding-related inaccessibility of the motif as well as due to unspecific binding. Therefore, this result of the peptide array is not conclusive. To circumvent ambiguities of the array, we decided to inactivate the potential LIR motifs altogether and to study them collectively. This allowed us to work out the selectivity for LC3B in HeLa cells (Figures 2 and S1C). Although LC3B is often considered the bona fide autophagy marker linking ubiquitin receptors and their cargo to the autophagosomal membrane, it is not strictly necessary for autophagosome formation or cargo recognition.[37] Indeed, other LC3s may very well compensate for a loss of LC3B.[37] Furthermore, the phagophore is not exclusively equipped with a single type of LC3. Still, LC3B and LC3C appear to work at opposing ends of the autophagic spectrum.[38,39] Notably, HeLa cells in general have a reportedly low expression of LC3C with 0.1 nTPM according to the human protein atlas (proteinatlas.org) project.[40] This might have compromised the traceability of an interaction with LC3C by the methods used. Further support for an LC3B selectivity might be provided by the peptide array, which likewise suggested the most intense binding for LC3B (Figure 1G). Collectively, our colocalization analysis regarding selectivity of a LIR-dependent interaction of BAG3 with LC3 proteins upon proteostasis stress suggests a preference for LC3B. A specific interference to LC3C was not ascertained (Figure S3B,D). Therefore, the ability of BAG3 to interact with at least LC3B underlines a potential function as an autophagy receptor.

We did not detect a significant LIR or treatment-specific effect on the proportional area of LC3 colocalizing BAG3 (Figure 2C). As discussed above, for example, a BafA1-induced increase in LC3B area or cargo-mediated translocation to autophagosomes without a direct BAG3–LC3 interaction might have impacts on changes in the relative proportion of BAG3 colocalizing with LC3. Comparison of the fluorescence intensity profiles of wild type versus ΔLIR-BAG3 within designated cell region indicated—although both paradigms showed a correlation—an elevated specificity of wild-type BAG3 towards LC3B-positive structures especially after BafA1-treatment (Figure 2B). To identify the specific effects, we looked at the enrichment of BAG3 (mean area of BAG3-positive puncta) within the LC3B-positive structures (Figure 2D). Here, a BafA1-inducible LIR dependency of the specific BAG3 enrichment became apparent. Whereas the concentration of wild-type BAG3 in LC3B-positive structures was significantly induced after BafA1 treatment, the absence of this effect for the

ΔLIR-BAG3 clearly indicated a LIR-dependent translocation to these structures (Figure 2D). The ΔLIR-BAG3 not only caused a collapse of the inducible BAG3 amount colocalizing in BAG3/LC3B-positive puncta, but furthermore massively decreased the quantity of BAG3 in autophagic vesicles (Figure 3E,F). Our data suggest that about half of the BAG3 present in autophagic vesicles in the context of the selected treatment could be LIR-dependent. The minor amounts of ΔLIR-BAG3 in autophagic vesicles might also be explained via a residual translocation by interactions beyond the LIRs as suggested by the peptide array or as part of the ternary complex, for example, with HSP70 including its cargo, targeted via classical autophagy receptors.

Previous data suggested that BAG3 may partake in autophagic processes independent of ubiquitin and may potentially also deal with non-ubiquitinated cargo.[8] Therefore, we also looked at the amount of BAG3 in autophagic vesicles in presence of PYR-41 and a disabled E1 ubiquitin ligase activity. Inhibition of ubiquitination by PYR-41 also resulted in a similar reduction of BAG3 as the ΔLIR mutant. Although the reduced levels post-PYR-41 treatment indicate preferential functionality for ubiquitinated cargo, a function for nonubiquitinated cargo cannot be excluded. Since we could not detect such an effect for ΔLIR-BAG3 (Figure 3G), the effects are likely not just additive. Ubiquitination events have very complex effects on, for instance, autophagosome maturation[41] and, as recently demonstrated, proteasome inhibition promote alternative pathways beyond autophagy towards lysosomal degradation.[42] Therefore a more detailed analysis beyond pharmacological inhibition of ubiquitination is required to reveal the functional aspects of ubiquitination-dependent amounts of BAG3 in autophagic vesicles.

In conclusion, our data strongly suggest that LIRs are required for efficient translocation of BAG3 into autophagosomes (Figure 3E,F). Here, we were able to identify an on demand interaction of BAG3 with LC3B in the context of upregulated BAG3-mediated selective macroautophagy pathway. Therefore, we hypothesize that a LIR-dependent translocation of BAG3 to autophagosomes may also affect sequestered HSP70 cargo and drive its autophagic degradation.

PEER REVIEW

The peer review history for this article is available at https://www.webofscience.com/api/gateway/wos/peer-review/10.1111/tra.12916.

DATA AVAILABILITY STATEMENT

All data are incorporated into the article and its online supporting information.

ORCID

Hagen Körschgen https://orcid.org/0000-0003-2802-2669
Christian Behl https://orcid.org/0000-0001-8453-2378

REFERENCES

1. Chiang H-L, Terlecky SR, Plant CP, Dice JF. A role for a 70-Kilodalton heat shock protein in lysosomal degradation of intracellular proteins. *Science*. 1989;246:382-385.
2. Kirchner P, Bourdenx M, Madrigal-Matute J, et al. Proteome-wide analysis of chaperone-mediated autophagy targeting motifs. *PLoS Biol*. 2019;17:e3000301.
3. Lüders J, Demand J, Höhfeld J. The ubiquitin-related BAG-1 provides a link between the molecular chaperones Hsc70/Hsp70 and the proteasome. *J Biol Chem*. 2000;275:4613-4617.
4. Kim YE, Hipp MS, Bracher A, Hayer-Hartl M, Ulrich Hartl F. Molecular chaperone functions in protein folding and Proteostasis. *Annu Rev Biochem*. 2013;82:323-355.
5. Garrido C, Paul C, Seigneuric R, Kampinga HH. The small heat shock proteins family: the long forgotten chaperones. *Int J Biochem Cell Biol*. 2012;44:1588-1592.
6. Gamerdinger M, Hajieva P, Kaya AM, Wolfrum U, Hartl FU, Behl C. Protein quality control during aging involves recruitment of the macroautophagy pathway by BAG3. *EMBO J*. 2009;28:889-901.
7. Takayama S, Xie Z, Reed JC. An evolutionarily conserved family of Hsp70/Hsc70 molecular chaperone regulators. *J Biol Chem*. 1999;274:781-786.
8. Gamerdinger M, Kaya AM, Wolfrum U, Clement AM, Behl C. BAG3 mediates chaperone-based aggresome-targeting and selective autophagy of misfolded proteins. *EMBO Rep*. 2011;12:149-156.
9. Meriin AB, Narayanan A, Meng L, et al. Hsp70–Bag3 complex is a hub for proteotoxicity-induced signaling that controls protein aggregation. *Proc Natl Acad Sci U S A*. 2018;115:E7043-E7052.
10. Carra S, Seguin SJ, Lambert H, Landry J. HspB8 chaperone activity toward poly(Q)-containing proteins depends on its association with Bag3, a stimulator of macroautophagy. *J Biol Chem*. 2008;283:1437-1444.
11. Klimek C, Kathage B, Wördehoff J, Höhfeld J. BAG3-mediated proteostasis at a glance. *J Cell Sci*. 2017;130:2781-2788.
12. Minoia M, Boncoraglio A, Vinet J, et al. BAG3 induces the sequestration of proteasomal clients into cytoplasmic puncta. *Autophagy*. 2014;10:1603-1621.
13. Korac J, Schaeffer V, Kovacevic I, et al. Ubiquitin-independent function of optineurin in autophagic clearance of protein aggregates. *J Cell Sci*. 2013;126:580-592.
14. Bjørkøy G, Lamark T, Brech A, et al. p62/SQSTM1 forms protein aggregates degraded by autophagy and has a protective effect on huntingtin-induced cell death. *J Cell Biol*. 2005;171:603-614.
15. Pankiv S, Clausen TH, Lamark T, et al. p62/SQSTM1 binds directly to Atg8/LC3 to facilitate degradation of Ubiquitinated protein aggregates by autophagy. *J Biol Chem*. 2007;282:24131-24145.
16. Ichimura Y, Kirisako T, Takao T, et al. A ubiquitin-like system mediates protein lipidation. *Nature*. 2000;408:488-492.
17. Birgisdottir ÅB, Lamark T, Johansen T. The LIR motif - crucial for selective autophagy. *J Cell Sci*. 2013;126:3237-3247.
18. Johansen T, Lamark T. Selective autophagy: ATG8 family proteins, LIR motifs and cargo receptors. *J Mol Biol*. 2020;432:80-103.
19. Lv M, Wang C, Li F, et al. Structural insights into the recognition of phosphorylated FUNDC1 by LC3B in mitophagy. *Protein Cell*. 2017;8:25-38.
20. Birgisdottir ÅB, Mouilleron S, Bhujabal Z, et al. Members of the autophagy class III phosphatidylinositol 3-kinase complex I interact with GABARAP and GABARAPL1 via LIR motifs. *Autophagy*. 2019;15:1333-1355.
21. Rogov VV, Suzuki H, Marinković M, et al. Phosphorylation of the mitochondrial autophagy receptor nix enhances its interaction with LC3 proteins. *Sci Rep*. 2017;7:1-12.
22. Keown JR, Black MM, Ferron A, et al. A helical LC3-interacting region mediates the interaction between the retroviral restriction factor Trim5α and mammalian autophagy-related ATG8 proteins. *J Biol Chem*. 2018;293:18378-18386.
23. Huber J, Obata M, Gruber J, et al. An atypical LIR motif within UBA5 (ubiquitin like modifier activating enzyme 5) interacts with GABARAP proteins and mediates membrane localization of UBA5. *Autophagy*. 2020;16:256-270.
24. von Muhlinen N, Akutsu M, Ravenhill BJ, et al. LC3C, bound selectively by a noncanonical LIR motif in NDP52, is required for antibacterial autophagy. *Mol Cell*. 2012;48:329-342.
25. Marshall RS, Hua Z, Mali S, McLoughlin F, Vierstra RD. ATG8-binding UIM proteins define a new class of autophagy adaptors and receptors. *Cell*. 2019;177:766 781.e24.
26. Wirth M, Zhang W, Razi M, et al. Molecular determinants regulating selective binding of autophagy adapters and receptors to ATG8 proteins. *Nat Commun*. 2019;10:2055.
27. Atkinson JM, Ye Y, Gebru MT, et al. Time-resolved FRET and NMR analyses reveal selective binding of peptides containing the LC3-interacting region to ATG8 family proteins. *J Biol Chem*. 2019;294:14033-14042.
28. Sora V, Kumar M, Maiani E, Lambrughi M, Tiberti M, Papaleo E. Structure and dynamics in the ATG8 family from experimental to computational techniques. *Front Cell Dev Biol*. 2020;8:1-28.
29. García-Mata R, Bebök Z, Sorscher EJ, Sztul ES. Characterization and dynamics of Aggresome formation by a cytosolic Gfp-chimera. *J Cell Biol*. 1999;146:1239-1254.
30. Baeken MW, Behl C. On the origin of BAG(3) and its consequences for an expansion of BAG3's role in protein homeostasis. *J Cell Biochem*. 2022;123:102-114.
31. Ran FA, Hsu PD, Wright J, Agarwala V, Scott DA, Zhang F. Genome engineering using the CRISPR-Cas9 system. *Nat Protoc*. 2013;8:2281-2308.
32. Schmitt D, Bozkurt S, Henning-Domres P, et al. Lipid and protein content profiling of isolated native autophagic vesicles. *EMBO Rep*. 2022;23:e53065. doi:10.15252/embr.202153065
33. Schindelin J, Arganda-Carreras I, Frise E, et al. Fiji: an open-source platform for biological-image analysis. *Nat Methods*. 2012;9:676-682.
34. Waterhouse A, Bertoni M, Bienert S, et al. SWISS-MODEL: homology modelling of protein structures and complexes. *Nucleic Acids Res*. 2018;46:W296-W303.
35. Pettersen EF, Goddard TD, Huang CC, et al. UCSF chimera? A visualization system for exploratory research and analysis. *J Comput Chem*. 2004;25:1605-1612.

36. Yang Y, Kitagaki J, Dai R-M, et al. Inhibitors of ubiquitin-activating enzyme (E1), a new class of potential cancer therapeutics. *Cancer Res*. 2007;67:9472-9481.

37. Baeken MW, Weckmann K, Diefenthäler P, et al. Novel insights into the cellular localization and regulation of the Autophagosomal proteins LC3A, LC3B and LC3C. *Cell*. 2020;9:2315.

38. Lamark T, Johansen T. Mechanisms of selective autophagy. *Annu Rev Cell Dev Biol*. 2021;37:143-169.

39. Varga VB, Keresztes F, Sigmond T, Vellai T, Kovács T. The evolutionary and functional divergence of the atg8 autophagy protein superfamily. *Biol Futur*. 2022;73:375-384. doi:10.1007/s42977-022-00123-6

40. Uhlen M, Zhang C, Lee S, et al. A pathology atlas of the human cancer transcriptome. *Science*. 2017;357:eaan2507. doi:10.1126/science.aan2507

41. Chen R-H, Chen Y-H, Huang T-Y. Ubiquitin-mediated regulation of autophagy. *J Biomed Sci*. 2019;26:80.

42. Goebel T, Mausbach S, Tuermer A, et al. Proteaphagy in mammalian cells can function independent of ATG5/ATG7. *Mol Cell Proteomics*. 2020;19:1120-1131.

SUPPORTING INFORMATION

Additional supporting information can be found online in the Supporting Information section at the end of this article.

How to cite this article: Körschgen H, Baeken M, Schmitt D, Nagel H, Behl C. Co-chaperone BAG3 enters autophagic pathway via its interaction with microtubule associated protein 1 light chain 3 beta. *Traffic*. 2023;24(12):564-575. doi:10.1111/tra.12916